

Quantification of Heat Flux from a Reacting Thermite Spray

2009 ASME Summer Heat Transfer Conference

Eric Nixon
Michelle Pantoya
Daniel Prentice

July 2009

The INL is a
U.S. Department of Energy
National Laboratory
operated by
Battelle Energy Alliance



This is a preprint of a paper intended for publication in a journal or proceedings. Since changes may be made before publication, this preprint should not be cited or reproduced without permission of the author. This document was prepared as an account of work sponsored by an agency of the United States Government. Neither the United States Government nor any agency thereof, or any of their employees, makes any warranty, expressed or implied, or assumes any legal liability or responsibility for any third party's use, or the results of such use, of any information, apparatus, product or process disclosed in this report, or represents that its use by such third party would not infringe privately owned rights. The views expressed in this paper are not necessarily those of the United States Government or the sponsoring agency.

HT2009-88219

QUANTIFICATION OF HEAT FLUX FROM A REACTING THERMITE SPRAY

Eric Nixon

Texas Tech University
Lubbock, TX USA

Michelle Pantoya

Texas Tech University
Lubbock, TX USA

Daniel Prentice

Idaho National Laboratory
Idaho Falls, ID USA

Abstract

Characterizing the combustion behaviors of energetic materials requires diagnostic tools that are often not readily or commercially available. For example, a jet of thermite spray provides a high temperature and pressure reaction that can also be highly corrosive and promote undesirable conditions for the survivability of any sensor. Developing a diagnostic to quantify heat flux from a thermite spray is the objective of this study. Quick response sensors such as thin film heat flux sensors can not survive the harsh conditions of the spray, but more rugged sensors lack the response time for the resolution desired. A sensor that will allow for adequate response time while surviving the entire test duration was constructed. The sensor outputs interior temperatures of the probes at known locations and utilizes an inverse heat conduction code to calculate heat flux values. The details of this device are discussed and illustrated. Temperature and heat flux measurements of various thermite spray conditions are reported. Results indicate that this newly developed energetic material heat flux sensor provides quantitative data with good repeatability.

Introduction

Although thermites have been used for a long time, the relatively recent development of nano scale thermites has opened the door to a new realm of possibilities. For example, nanoparticles demonstrate reduced ignition delay times and increased reaction speeds [1]. The unique combustion behaviors have inspired an application involving the use of a nozzle to produce a jet of thermite spray. A thorough literature investigation has revealed no reported heat transfer characteristics of a thermite spray. One explanation for this lack of understanding may be because nanoparticles significantly enhance the ease at which a spray can be generated, and the advent of nanoparticle technology is relatively new. Another explanation is that the diagnostic

capacity to measure heating rate and flux are not off-the-shelf and therefore not readily available to the average researcher. The objective of this study is to develop a calorimeter sensor to quantify heat flow from a reacting thermite spray and develop an apparatus that produces a thermite spray using fundamental flame spray concepts. The approach used to measure heat flux is somewhat similar to an approach utilized by White et al. [2] in which quasi steady state heat flux is determined, from an aluminum seeded hydrocarbon flame spray.

Sensor Development

The heat flux sensor design includes 316 stainless steel rods and plating, aluminum housing, lead-free solder, insulation and thermocouples. The stainless steel rods act as probes and are fitted with multiple thermocouples. The variation in temperature with distance along the probe allows the surface heat flux and surface temperature to be determined. The analysis is detailed in the Results and Discussion section.

To measure the surface heat flux and temperature profiles, multiple probes were used. Each probe provides temperature data at a specific location with respect to a stainless steel faceplate (Figure 1). Each probe size is 3.175 mm diameter and approximately 70 mm long. The chosen length allows a semi-infinite rod length assumption to be made for the entire time of interest. The spacing between the probe centers are all held at 7.62 mm. The locations of the probes on the surface plate can be seen in Figure 1.

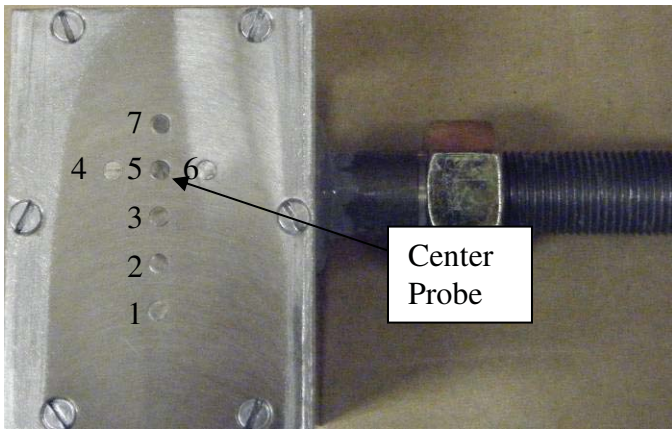


Figure 1 – Probe arrangement on stainless steel faceplate with each probe location numbered.

The probes immediately surrounding the center probe can be used to determine surface heat flux and temperature symmetry about the center probe. When heat flux is not axisymmetric, these probes can be used to create an approximate heat flux profile within a 7.62 mm radius of the center probe. For scenarios where symmetry about the center probe exists, the center probe along with the three probes below the center probe allow for an approximated heat flux and surface temperature profile with a radius of 22.86 mm from the center probe. There is a small gap between the edge of each probe and the plate of 0.0127 mm. All probes are flush with the surface plate. The surface plate and the probe ends are milled to be flat and smooth. This minimizes fluid flow disturbances from uneven heights, surface roughness and the presence of the probes themselves.

The thickness of the 316 stainless steel plate within a diameter of 6.350 mm about each probe is between 0.254 and 0.381 mm as shown in figure 2. This creates a contact resistance of 126.6 (K/W) to 189.8 (K/W) in the radial direction¹ [3]. The plate thickness in this region is a trade off to provide sufficient strength around the probes for pressure and thermal loading, while remaining relatively thin to minimize conduction in the radial direction. The remaining plate thickness around the probes is 6.35 mm.

The front plate is connected and secured to the aluminum housing with dimensions of 57.15x50.165x69.85 mm. The walls are 6.35 mm thick, which leaves a 44.45x37.465x63.5 mm void space within the instrument. This space is filled with Cotronics 740 series alumina silica insulation foam which has a thermal conductivity of 1 BTU-in/hr-R-ft² or 0.1442 W/m-K².

Every probe has 0.0762 mm diameter type E thermocouples secured in three locations; at 0.889, 12.827 and 50.8 mm from the probe tip. Each thermocouple location was notched on both the top and bottom of the side of the rod with a 90 degree V-notch milled to 0.3556 mm wide and 0.1778 mm deep. This size notch was chosen to allow the thermocouple wire to be fully encased in solder while minimizing the thermal disturbance created by the presence of the thermocouple.

A calibration test was performed on each probe from 25 to 200° C at atmospheric pressure using an Imperial V laboratory oven. These calibrations check voltages at corresponding temperatures and it was found that the voltages do not vary from the output voltages produced from an unmodified factory thermocouple. It was found that the thermocouples vary less than one degree with respect to the other probe thermocouples at a given oven temperature.

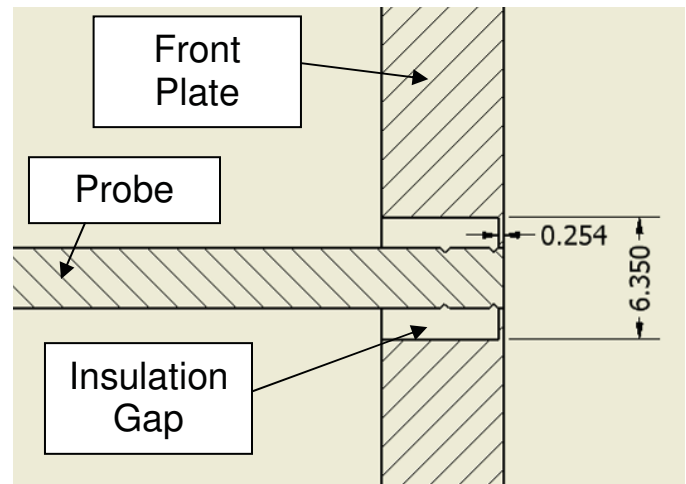


Figure 2 - Section view of face plate and probe to illustrate plate dimensions.

Thermite Spray Apparatus

The thermite is contained in an acrylic liner with a volume of 0.890 cm³ which is in turn incased within a 50.8 mm outer diameter phenolic rod (McMaster-Carr Garolite grade G-10). The nozzle for the thermite spray is constructed of the same phenolic material. The conic section has dimensions of a base width of 10.16 mm, a top diameter of 1.70 mm and height of 4.23 mm which yields a base over height ratio of 2. This ratio was chosen as a middle starting point for testing equivalence ratios. The orifice diameter is 1.7018 mm and the length is 3.40 mm. Figure 3 provides visual clarification of the geometry of the nozzle.

1. Thermal conductivity of air based on 300K at atmospheric pressure

2. Thermal conductivity values based on manufacturer's data.

http://www.cotronics.com/vo/cotr/cm_castable.htm

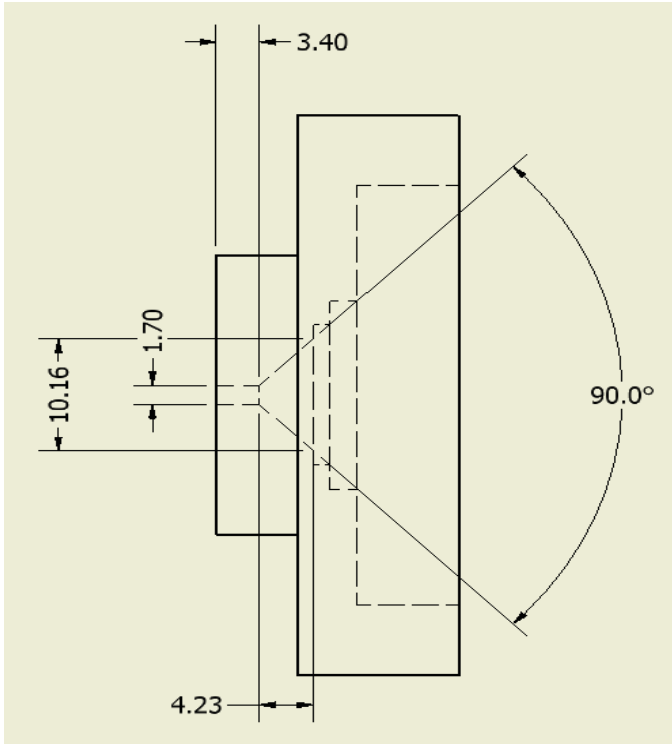


Figure 3 – The geometry of the thermite spray nozzle.

The thermite mixture is composed of 80 nm Al from Nanotechnologies, Inc. mixed with 30-50 nm CuO from Alfa Aesar. The total mass for each test is held constant at 250 ± 0.5 mg. Respective amounts of each powder are measured on a scale with 0.1 mg accuracy and are based on the equivalence ratio, which is defined in equation 1.

$$\Phi = \frac{m_{fuel} / m_{oxidizer}}{\left(m_{fuel} / m_{oxidizer} \right)_{st}} \quad (1)$$

The bottom fuel to oxidizer ratio is the stoichiometric ratio. Hexane is added to the powders and a sonicator is used to mix the powders to a homogeneous mixture. The hexane is then evaporated off and the powders are reclaimed. 250 mg of powder mixture is then added to the acrylic liner. The powder is left loosely packed, maintaining a constant bulk density for each experiment.

The nozzle is placed over the acrylic liner double o-ring seals aid in avoiding pressure leaks during the reaction. These seals are seen in figure 4.

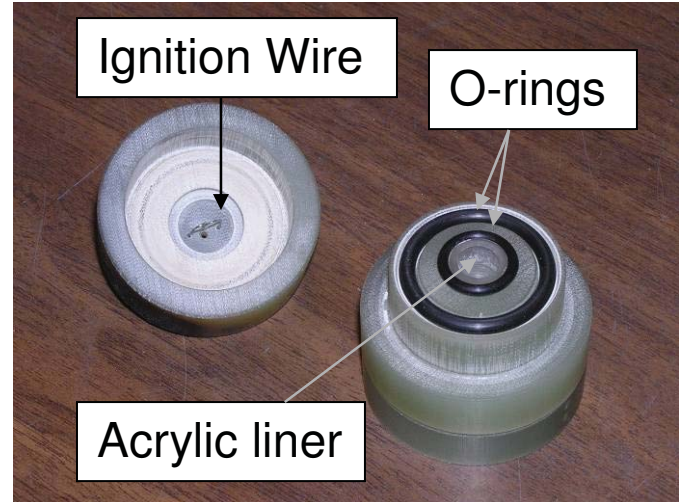


Figure 4 – Nozzle with ignition wire and base that contains the thermite.

The ignition source for the thermite was resistance heating through a nichrome wire as shown in figure 4. The voltage to this wire was controlled with a variac transformer. The assembled nozzle and base was then clamped into the testing apparatus. Figure 5a shows the testing apparatus and figure 5b shows the setup as it appears just before ignition. The distance between the nozzle tip and heat flux sensor is 26.67 mm.

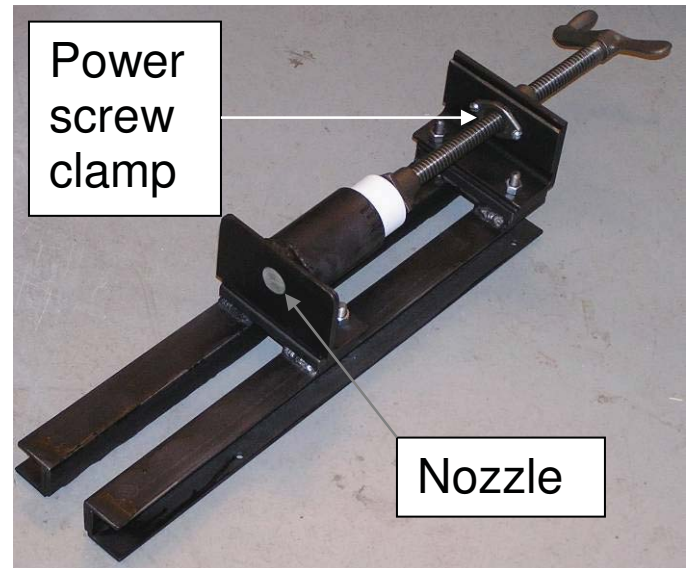


Figure 5a – Thermite spray apparatus without temperature probes.

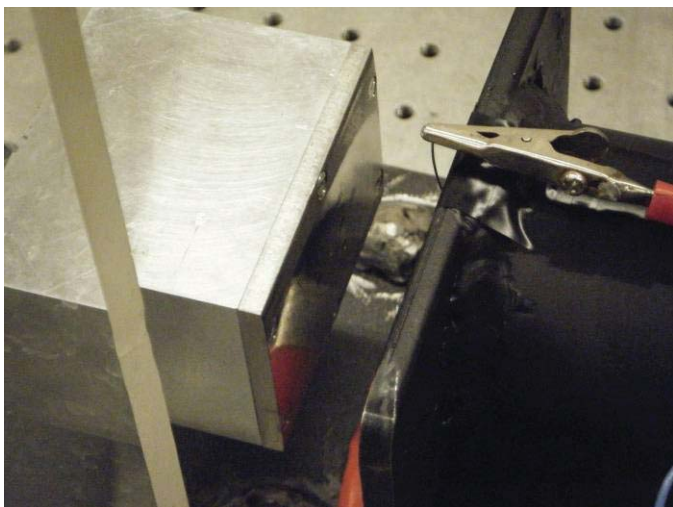


Figure 5b – Heat flux sensor shown with thermite spray apparatus.

A Phantom 7 high speed camera was used to record the reaction at a frame rate of 40,000 frames per second (fps). The camera was positioned such that its viewing direction is orthogonal to the direction of the spray. This angle allowed for the burn time and initial flame front velocity to be measured from photographic data.

Each thermocouple used during a test was connected to an InstruNet 100B external data acquisition system (DAQ). The DAQ used contains signal conditioning amplifiers and analog filters that allow for direct connection with thermocouples. Due to the hardware limitations of the data acquisition system, a maximum of 5 temperature probes can be used during a test. A sample frequency of 250 Hz with an integration time or moving average time of $1/6000^{\text{th}}$ of a second was used. The integration time was the first noise filter used. The second filter used was an analog 40Hz low pass filter selected from the hardware settings of the InstruNet software.

A photodiode was used to identify the time of first light which corresponds to time zero. The photodiode is connected to the InstruNet DAQ so that the photodiode and thermocouple data coincide.

In addition to high speed video and temperature data, a high speed infrared camera (Phoenix MWIR from FLIR Systems) provided qualitative information about the thermal distribution on the plate surface following the reaction.

Results

The first test determined if the heat flux and temperature was axisymmetric about the center probe. For this test, 250 mg of Al + CuO was used at an equivalence ratio of one. The internal temperatures from the front thermocouple in each probe are shown in figure 6. Temperature distributions captured by the infrared camera are shown in figure 7. The temperature distributions seen in this figure also indicate

symmetry about the center probe. It should be noted that the two ‘hot spots’ seen on the corners of the plate in figure 7 are surface reflections of the nichrome ignition wire and should be disregarded.

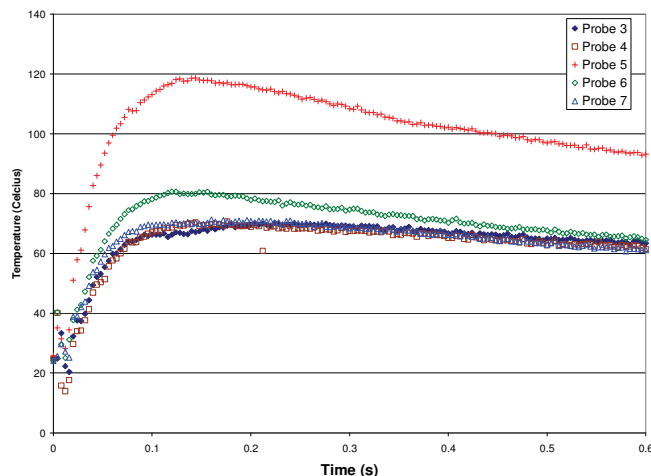


Figure 6 – Internal temperatures for axisymmetric test using center and surrounding probes.

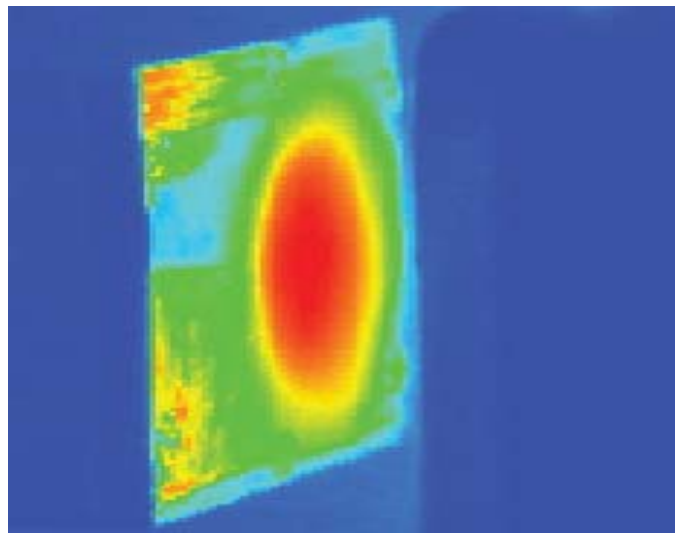


Figure 7 – Surface temperatures captured on the face plate with the infrared camera.

The next set of experiments examined the variation in equivalence ratio for stoichiometric to fuel rich, $\Phi=1$, $\Phi=1.2$, and $\Phi=1.4$.

Video from each equivalence ratio showed that the initial flame speeds are independent of equivalence ratio and are measured to be $139 \text{ m/s} \pm 15 \text{ m/s}$. Flame velocities after the initial flame speed are difficult to determine due to a lack of identifiable reference points. However, approximated burn times appear to be relatively constant as well. Total spray times for the various equivalence ratios range from 40 to 60 ms. Given that the total mass was held constant and the

nozzle geometry was not changed, an assumption can be made that the mass flow rates as well as velocities should be consistent for each equivalence ratio. Figure 8 shows still images of the thermite spray at various times during the reaction.

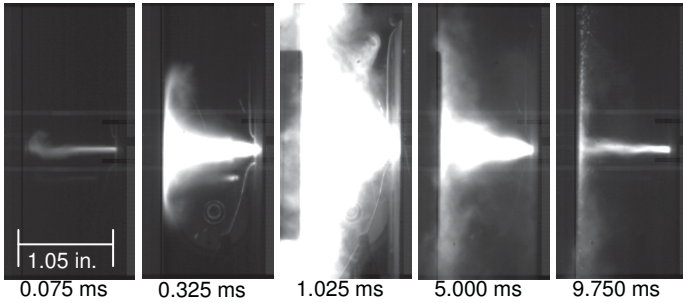


Figure 8 – Still images of reaction at $\Phi=1.2$.

Figure 9 shows a comparison of the front most thermocouple at the center probe. Due to space limitations, only the center probe is shown.

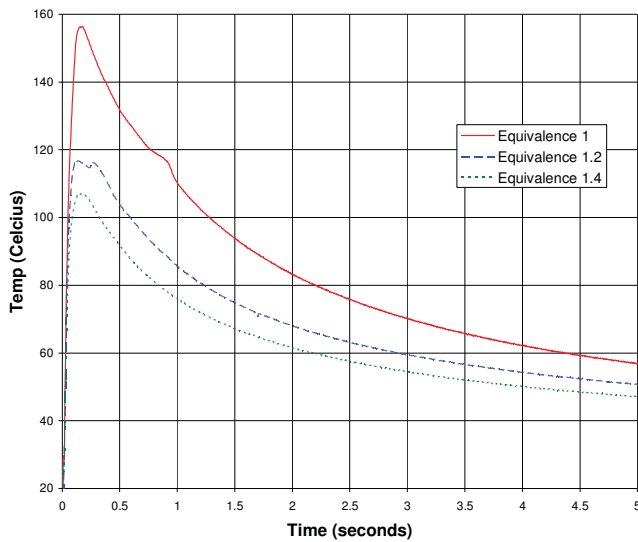


Figure 9 – Comparison of front thermocouple temperatures of the center probe at various equivalence ratios

Before any calculations for surface heat flux and temperatures could be performed, a third data filter was found to be very useful for removing additional thermocouple noise. This filter, as opposed to the first two filters which are applied to the data before it is recorded, is actually applied to the raw data itself. Figure 10 shows a magnified view of the peak temperature of the center probe for an equivalence ratio of 1. This specific point was chosen because this small region contained the largest temperature gradients within all the data sets.

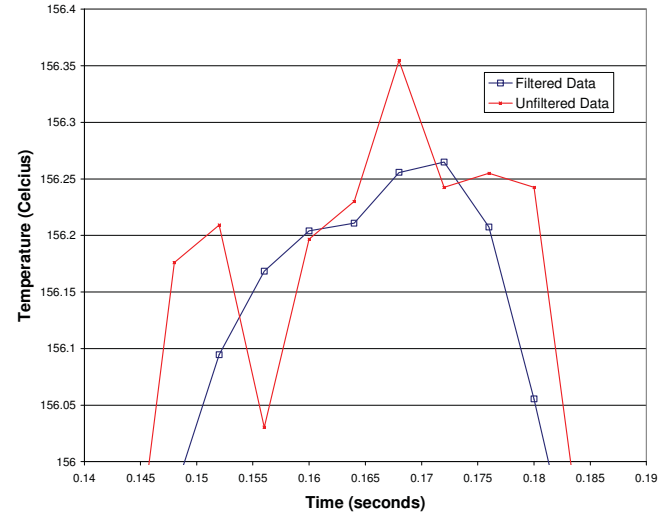


Figure 10 – Effect of numerical filter on data noise oscillations

The filter used here is a series of five point linear curve fits that use the $n-2^{\text{th}}$, $n-1^{\text{th}}$, n^{th} , $n+1^{\text{th}}$ and $n+2^{\text{th}}$ data points. The new location of the point is found by using the time of the n^{th} point in the equation of the linear curve fit. As long as a sufficiently large sample rate is used, this technique creates a data ‘smoothing’ effect without losing important information regarding ‘temperature spikes’.

After the third filter, a commercial inverse heat transfer analysis software package (IHCPID) from Beck Engineering Consultants, Inc. was utilized to calculate the surface temperature and heat flux. This code calculates the heat flux and temperature in the inverse region (between surface and first interior temperature) by using a subsequent least squares procedure until the calculated temperatures agree in a least squares sense with the measured temperatures [4]. The temperatures involved in each least squares calculation for any time step includes the current temperature and a user specified number of future time steps. The number of future time steps needed is dependent on the particular data set and is determined iteratively. The residuals (difference between the measured and calculated temperatures), standard deviation of the residuals, and the general shape of the estimated data curves are taken into account to determine the best approximation for the surface heat flux and temperature. Results of the code for the equivalence ratio of 1 test are shown in figures 11 and 12.

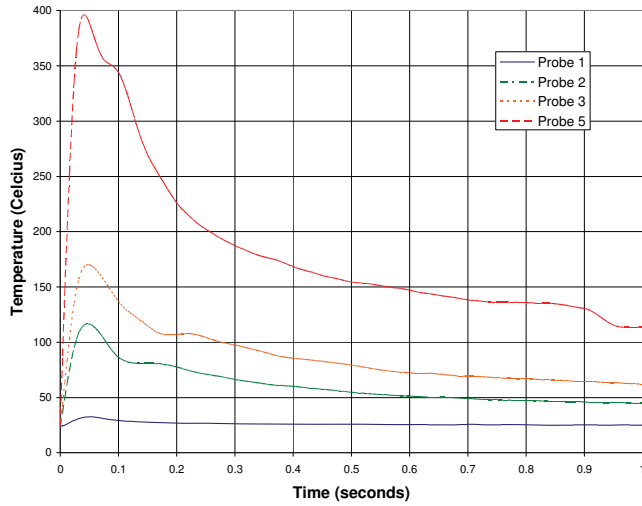


Figure 11 – Surface temperature of 250 mg Al + CuO at $\Phi=1$.

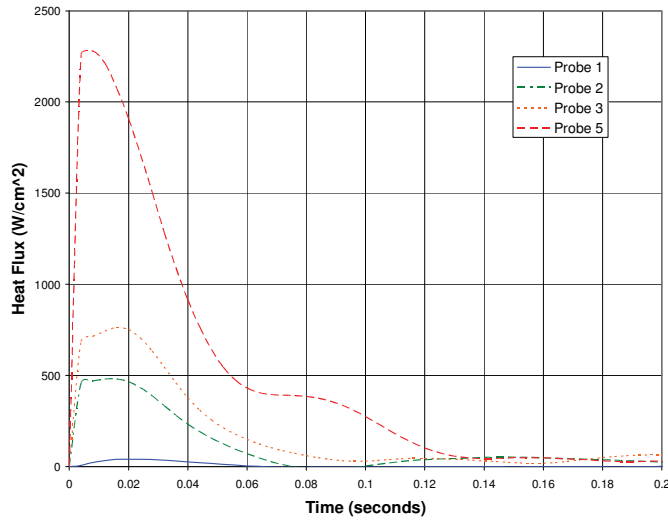


Figure 12 – Surface heat flux of 250 mg Al + CuO at $\Phi=1$.

To validate the numerical results from the software, an explicit one dimensional transient heat conduction scheme with order of accuracy of $O(\Delta t) + O[(\Delta x)^2]$ was used. This scheme was written into an algorithm that uses the surface temperature and heat flux for one boundary condition and the known temperature at the other boundary. The algorithm allows the user to select spatial and temporal step sizes via the number of nodes and a Fourier number. Both values were adjusted until convergence was achieved. The temperature differences between measured and calculated interior temperatures are shown in figure 13.

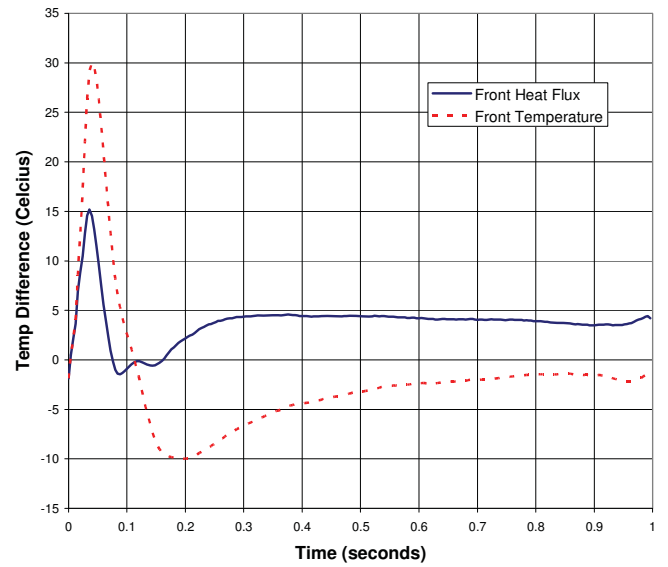


Figure 13 – Temperature differences between the measured and calculated values of the temperature of the front thermocouple in the center probe.

The energy per unit area for each probe location was determined by taking the area under the curve in figure 12. The energy distribution as a function of equivalence ratio can be seen in figure 14.

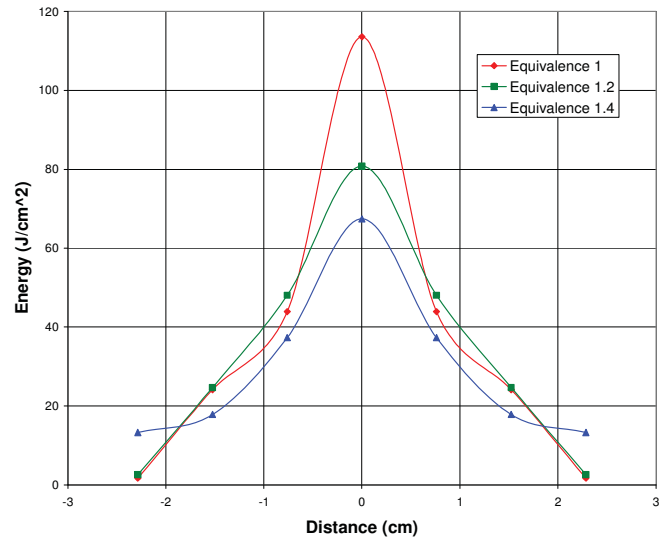


Figure 14 – Total energy per unit area measured.

By approximating the energy distribution between data points with linear lines, and using the shell method, the total energy within a radius of 22.9 mm from the center probe was determined. This information is presented in table 1.

Efficiency Measurements			
	Equivalence 1	Equivalence 1.2	Equivalence 1.4
E_{in} Plate (J)	413.3	416.9	371.9
$\Delta h_{combustion}$ $2Al + 3CuO \rightarrow Al_2O_3 + 3Cu$	983.0	941.7	903.6
$\Delta h_{combustion}$ $2Al + 3O_2 \rightarrow 2Al_2O_3$	0.0	262.2	503.1
Lower Efficiency	42.04%	34.63%	26.44%
Upper Efficiency	42.04%	44.28%	41.16%

Table 1 – Comparison of energy absorbed by the front plate and the potential energy released from the reaction

The efficiency of the thermite spray is based upon the energy released from the reaction. It is assumed that all of the CuO reacts with the aluminum. For the fuel rich tests, an upper and lower efficiency value is established based upon the excess aluminum reacting with air (lower efficiency value) or if none of the excess aluminum reacts (upper efficiency value).

Discussion

It can be concluded from inspection of figure 6 that this setup produces axisymmetric results. This is to be expected as the orifice of the nozzle is directly in line with the center probe, and as a result receives the greatest convective heating. In addition, the time scale of the reaction and the initial flame front velocity would allow a reasonable assumption that any natural convection or buoyancy effects of the hot products would be relatively small with respect to the forced convection and therefore neglected.

The temperature disturbances created by the presence of the thermocouple wires and soldered notch are neglected in the analysis since the wire size and notch are small in comparison to the probe dimensions. Small temperature oscillations are amplified in the inverse region of the numerical analysis as a result of differentiation of the experimental data. As a larger number of future time steps are used, the calculated results become more stable. However, when regions of quick changes in surface heat flux and surface temperature exist, more future time steps lead to greater numerical diffusion, which in turn will lead to understating the peak heat flux and temperature values.

These values shown in figure 13 are positive differences between the measured and calculated internal temperatures at the beginning of the graph, indicating that surface temperature and heat flux values shown earlier are understated, and conservative numbers. Understatements of the values are unavoidable within this first region since numerical diffusion is unavoidable.

The energy distribution seen in figure 14 shows that as the thermite becomes more fuel rich, the total energy absorbed from the center of the spray decreases. One possible explanation could be that the excess fuel has not reacted. Table 1 indicates that equivalence ratios 1 and 1.2 result in similar quantities of energy absorbed while equivalence ratio 1.4 decreases. If achieving the highest energy density is the objective of the thermite spray, an equivalence ratio of 1 would be the most desirable ratio for a fixed total mass.

The uncertainty associated with the measured temperatures is primary driven by random measurement error and position. To account for random error as well as numerical error, a standard deviation of the differences between measured and calculated temperatures from 0 to 1 second (figure 13) is used. The random error is often amplified when performing an inverse heat conduction analysis, and therefore, this value should provide a conservative estimate. To normalize the probes, the standard deviation is divided by the maximum overall temperature change. The uncertainty of the heat flux can be expressed as:

$$\frac{u_{q''}}{q''} = \sqrt{\left(\frac{u_T}{\Delta T}\right)^2 + \left(\frac{u_x}{x}\right)^2} \quad (2)$$

where q'' is the heat flux, u_T is the temperature standard deviation already mentioned, ΔT is the maximum temperature change, u_x is the position uncertainty and x the distance from the surface to the thermocouple. Since the surface temperature is a convenient by-product of the surface heat flux, the surface temperature uncertainty normalized by the surface temperature would have the same value as the normalized heat flux uncertainty. This value was determined to be 10.3%.

Conclusion

The need for a diagnostic technique for quantification of a thermite spray was presented along with some test results used to validate the diagnostic technique. The approach was to utilize interior temperatures, which protected the thermocouples from damage, and employ an inverse heat conduction code to provide reasonable estimations of surface heat flux and temperature. Details of the equipment used along with necessary steps taken to address and minimize noise were discussed. A commercial code along with an algorithm to validate the results of the code was employed. The methodology and approach used were shown to provide reasonable results for situations in which quick response time is needed in a 'hostile' testing environment. The simplicity of this approach can be seen to have potential for a variety of other applications as well.

Acknowledgements

Technical and financial assistance for this work were provided by Idaho National Laboratory (INL). INL is a multiprogram laboratory operated by Battelle Energy Alliance for the United States Department of Energy. Dr. Pantoya also gratefully acknowledges support from the Army Research Office contract number W911NF-04-1-0217 and Dr. Ralph Anthenien.

References

- [1] Bockmon, B.S., Pantoya, M.L., Son, S.F., Asay, B.W., and Mang, J.T., 2005, "Combustion velocities and propagation mechanisms of metastable interstitial composites," *Journal of Applied Physics*, 98(6) pp. 064903-1-064903-7.
- [2] White, R.B., Dean, S.W., Pantoya, M.L., Hirschfeld, D.A., Gill, W., and Erikson, W.W., 2007, "Effect of aluminum on heat flux from a simulated rocket propellant flame," *Journal of Propulsion and Power*, 23(6) pp. 1255-1262.
- [3] Incropera, F.P., DeWitt, D.P., Bergman, T.L., and Lavine, A.S., *Fundamentals of Heat and Mass Transfer*, 2006, John Wiley and Sons, Inc., pp. 931-941.
- [4] Beck, J.V., *USER'S MANUAL FOR IHCPID*, 2006, Beck Engineering Consultants Company